J Mater Sci (2009) 44:1923–1933
DOI 10.1007/s10853-008-2888-3

INTERFACE SCIENCE

Dynamic wetting and heat transfer at the initiation of aluminum solidification on copper substrates

Dominique Bouchard · Sébastien Leboeuf · Jean-Paul Nadeau · Roderick I. L. Guthrie · Mihaiela Isac

Received: 27 July 2007 / Accepted: 18 July 2008 / Published online: 17 September 2008

Abstract Dynamic wetting and heat transfer during the start of solidification were studied with the help of molten aluminum droplets falling from a crucible onto a copper substrate. A high-speed camera captured the change in the spreading droplet's geometry, while thermocouple, inserted inside the substrate, allowed a heat transfer analysis to be performed. Droplet spreading factors and interfacial heat fluxes were then used to, respectively, characterize dynamic wetting and heat transfer for the various experimental conditions explored. These were: (1) effects of chemical composition of the aluminum alloy, (2) initial temperature of the substrate, (3) surface roughness of the substrate, and (4) composition of the gaseous atmosphere. The experiments were all carried out in gaseous atmospheres containing oxygen in sufficient amount to form oxide skins at the surface of the droplets and the substrates. The results showed instances where an improvement in the dynamic wetting was accompanied by an increase in heat transfer during the early stages of solidification but this was not systematic. In these cases where a positive correlation was not observed, it was postulated this was caused by factors such as variations in the oxidation at the surface of the substrates and the droplets as well as gas trapped at the interface between the droplets and the substrates.

Sébastien Leboeuf formerly with the Aluminum Technology Centre and McGill University.

D. Bouchard (✉) · J.-P. Nadeau
Aluminum Technology Centre, National Research Council, Canada, 501 boul. de l'Université, Chicoutimi, Québec, Canada G7H 8C3
e-mail: dominique.bouchard@cnrc-nrc.gc.ca

S. Leboeuf
Arvida Research and Development Centre, Rio Tinto Alcan Inc, 1950 Mellon Blvd, P.O. Box 1250, Jonquière, Québec, Canada G7S 4K8

R. I. L. Guthrie · M. Isac
McGill Metals Processing Centre, McGill University, 3610 University Street, M.H. Wong Building, Montréal, Québec, Canada H3A 2B2

Nomenclature

C	Heat capacity (kJ kg^{-1} K^{-1})
d	Droplet diameter (m)
E_K	Kinetic energy (J)
E_{surf}	Surface energy (J)
h	Height of fall (m)
i	Node identification in the numerical analysis
J	Total number of thermocouples
k	Thermal conductivity (W m^{-1} K^{-1})
m	Number of time intervals for inverse calculations or droplet mass (kg)
n	Iteration number in Eqs. 6 and 7
N	Total number of nodes
q	Interfacial heat flux per unit area (W m^{-2})
t	Time (s)
T	Temperature (K)
T_o	Initial temperature (K)
r	Number of future time-steps
v	Velocity (m/s)
We	Weber number
x	Length (m)
Y	Measured temperatures (K)
Z	Sensitivity coefficient (W K m^{-2})
δ	Incremental heat flux factor
γ	Surface tension (N m^{-1})
θ	Contact angle
ρ	Density (kg m^{-3})

σ Surface energy (J m^{-2})
ξ Spreading factor

Introduction

Wetting and heat transfer are two important phenomena occurring as metals begin to freeze on colder substrates. At this early stage, the wetting is a short-lived dynamic process occurring in a system out of thermodynamic equilibrium under highly transient heat transfer conditions. Improper dynamic wetting and/or heat transfer can result in non-uniform solidification and surface cracks [1]. The understanding and control of these two phenomena can find applications in rapid solidification processes [2] such as strip casting, thermal spraying, and laser cladding, as well as less rapid ones such as permanent mold and direct-chill (DC) casting since the initiation of solidification is also usually rapid. In some instances, dynamic wetting and heat transfer play a major impact not only on the surface quality of the product but also on the productivity of the process.

In principle, testing different parameters directly on an industrial process would allow one to find the optimal conditions for dynamic wetting and heat transfer, but each trial would be costly. An alternative is to build a test rig that can reproduce many of the conditions found at the start of solidification. Several such studies have been reported but these have focused on either dynamic wetting or heat transfer but not both. A brief overview is given below.

With dynamic wetting, Adler and Hsu [3] were among the first to acknowledge its importance in solidification processes. Their experimental approach, based on drop-splat experiments, produced droplets of various compositions that impacted on a copper substrate after a short free-fall. The use of a high-speed camera allowed the phenomena to be observed. Tests with copper, zirconium, and aluminum droplets were carried out, allowing dynamic wetting to be classified and showing the viability of this approach to find valid melt/substrate combinations for rapid solidification processes. Maringer [4] also used drop-splat experiments to study rapid solidification and reported "critical temperatures'' for which falling droplets (tin, aluminum, and zinc) would stick to an inclined substrate (copper, aluminum, and steel).

Dong et al. [1] also used drop-splat experiments to study the deformation of melts (pure Pb, Bi, Sn, and various alloys) on a copper substrate during solidification. They analyzed this phenomenon using a camera operating at 500–1000 frames/s and concluded that the instantaneous deformations of solidifying metals could explain the presence of certain defects on the cast surfaces. Ebrill et al. [5–8] studied dynamic wetting using a similar set-up to study hot dip coatings for steel sheets, while other authors working in the field of thermal spray coatings used it to study the interaction of molten metal with cooled substrates [9–12]. Megaridis et al. [13] studied dynamic wetting of Sn–Pb droplets impacting on a silicon substrate. Conditions whereby partial rebound of the droplets occurred were observed and a good agreement between the measurements and two predictive models for maximum lateral spread was reported.

Many studies have been carried out with non-metallic materials. It is not in the scope of this paper to present an overview of these works and only two noteworthy studies are cited here. Schiaffino and Sonin [14] examined the contact line motion of wax microdroplets that built-up and solidified on substrates of the same material. They reported that the contact line is arrested at an apparent contact angle that depended on the Stefan number. Prior to the arrest, the motion of the contact line appeared to obey the Hoffman-Tanner-Voinov law. Working with droplets of low viscosity fluids such as ethanol, methanol, and acetone, impinging on microscope glass slides, Rioboo et al. [15] reported that partial rebound of the droplets occurred in the complete wetting regime when low impact inertia simultaneously occurred with a high position of the center of mass of the droplet before spreading. Two dimensionless numbers were created to characterize the partial rebound.

In the aforementioned studies, three methods were employed to evaluate dynamic wetting: (1) apparent contact angles [5–8, 10, 13], (2) adherence forces [3, 4], and (3) spreading factors [9, 10, 12]. A vast amount of work with the sessile drop method has also been published; see for example the compilation by Eustathopoulos et al. [16]. These results are not discussed in this paper since they were usually obtained at, or close to, thermodynamic equilibrium, which is not representative of conditions prevailing at the initiation of solidification.

The drop-splat experiment has also been used to characterize the interfacial heat transfer between a solidifying metal and a substrate. Liu et al. [17, 18] and Wang and Matthys [19] used an electromagnetic levitator to melt nickel droplets and examined the cooling rates and interfacial heat transfer as these droplets solidified on substrates. Todoroki et al. [20–22] also carried out drop-splat experiments with steel and nickel and evaluated interfacial heat transfer coefficients along with heat fluxes. They pointed out that the maximum heat flux was highly dependent on the impingement location of the droplet with respect to the thermocouple. With a version of the set-up used by Todoroki et al., Misra et al. [23] demonstrated that a liquid oxide film such as FeO at the substrate/droplet interface can improve the contact between the two and significantly increase the rate of heat transfer during the first 20 ms of contact.

Loulou et al. [24, 25] used a dropt-splat set-up to evaluate heat fluxes and were among the first to attempt correlating wetting with heat transfer. They reported that metals with lower surface tensions and contact angles provided better heat transfer. However, the surface tension and contact angles values were taken from other publications and were not measured simultaneously with the heat transfer. Evans and Strezov [26] used a levitation apparatus to melt 0.7 g steel droplets and showed that an increase in the surface tension of steel droplets was associated with a decrease in the maximum heat fluxes.

In this work, drop-splat experiments were carried out to simultaneously study dynamic wetting and heat transfer, to investigate relationships between the two and more specifically, to determine if a large degree of droplet spreading would correlate with a large heat flux. There is indirect evidence that this may be the case through the work reported in references [23–26] but there is clearly a need for more experimental data. The experiments were carried out with aluminum droplets impinging on a copper substrate. Oxygen was present in the gas phase in sufficient amount to produce an oxide film at the surface of the droplet and the substrate. The affinity of aluminum for oxygen is such that virtually all metallurgical processes that involve its solidification are carried out in the presence of oxide films. The factors that were studied were: alloy composition, initial substrate temperature, substrate surface roughness, and gaseous atmospheres. This work, conducted at the Aluminum Technology Center, is a follow-up of a previous study that showed that increasing the height of fall of a droplet delayed the time at which the spreading was completed and that the time scale for spreading was of the same order as the one for the heat flux to reach a peak [27].

Theory

Characterization of dynamic wetting

In this study "spreading factors", (ξ), were used to characterize dynamic wetting. This factor is a measure of the flattening of the droplet obtained by the ratio of its final and initial diameters:

$$\text{Spreading factor} = \xi = \frac{d_f}{d_i} \tag{1}$$

As shown in Fig. 1, the initial diameter (d_i) refers to the one prevailing prior the impingement of the droplet on the substrate whereas the final diameter (d_f) refers to the one present once the droplet has completely spread.

The evaluation of these spreading factors provided a convenient characterization of dynamic wetting and has also been used in several other studies, for instance in the field of thermal spray coatings [9, 10, 12]. In addition, Ebrill et al. [5] demonstrated that with drop-splat experiments, the spreading factor was highly correlated with the final contact angle of dynamic wetting, (θ in Fig. 1), the former increasing as the latter decreased.

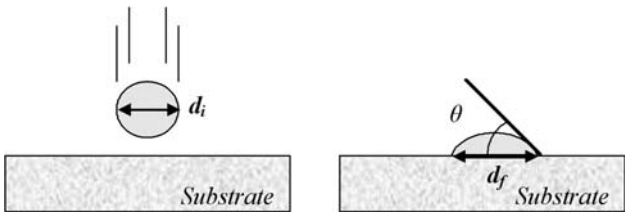

Fig. 1 Schematic illustration of the initial diameter (d_i) and final diameter (d_f) used to calculate the spreading factor. The contact angle is represented by θ

The dimensionless Weber number, *We*, is in this study useful to analyze the relative importance of the droplet inertia to its surface tension [28] and to identify some of the experimental parameters that can affect the results. This number is expressed as follows:

$$\frac{|\text{Inertia force}|}{|\text{Surface tension force}|} \propto \frac{\rho d v^2}{\gamma_{lg}} = We. \tag{2}$$

Assuming a droplet having a spherical shape and falling with no initial velocity, the Weber number can be rewritten as:

$$We = \frac{2\rho g h \left(\frac{6m}{\pi\rho}\right)^{1/3}}{\gamma_{lg}}. \tag{3}$$

It can be observed that in these experiments the height of fall of the droplet and its mass should be minimized for surface tension to play a relevant role. The ratio of the kinetic energy, E_K, of the droplet to its surface energy, E_{surf}, has also been used to estimate the extent of external perturbations to the wetting process [16]. For a droplet falling under gravity, the ratio of the kinetic energy to the surface energy is given by:

$$\frac{E_K}{E_{surf}} = \frac{\frac{1}{2}mv^2}{4\pi\sigma_{lg}r^2} = \frac{mgh}{\pi^{1/3}\sigma_{lg}\left(\frac{6m}{\rho}\right)^{2/3}}. \tag{4}$$

This ratio also shows that mass and height of fall need to be minimized for surface energy to be relevant. Other dimensionless numbers such as Reynolds, Froude, Bond, and Ohnesorge, have been used to characterize the deposition behavior of metal droplets [13]. See also [29] where dimensionless numbers were used to analyze spray forming, a process where droplet velocity is much greater than in drop-splat experiments.

Characterization of heat transfer

The energy released by the aluminum droplets after impingement was mainly by heat conduction into the substrate and was assumed to be primarily one-dimensional, as in the work of Todoroki et al. [21]. The 1D transient heat conduction equation in Cartesian coordinates is the following:

$$\frac{\partial}{\partial x}\left(k\frac{\partial T}{\partial x}\right) = \rho C\frac{\partial T}{\partial t}. \tag{5}$$

The above equation needs to be solved to characterize the heat flow and requires initial and boundary conditions, respectively, given in this work by:

$$T(x,0) = T_{\mathrm{o}} \qquad 0 \le x \le \infty \tag{6}$$

$$T(N,t) = T_{\mathrm{measured}} \qquad t \ge 0 \tag{7}$$

$$-k\frac{\partial T}{\partial x}\bigg|_{x=0} = q(t) \qquad t \ge 0 \tag{8}$$

The boundary condition of Eq. 7 states that the temperature at location N needs to be provided (Dirichlet condition). This was accomplished by imbedding a thermocouple a few millimeters below the surface of the substrate as described in greater details in the next section. Consequently, the calculations assumed the heat flow in the substrate was unidirectional to a depth corresponding to the location of that thermocouple. The thermophysical properties of copper used in the calculations are listed in Table 1.

The explicit finite difference approximations for the substrate temperatures derived from Eq. 5 are given in Table 2. The temperature evolution in the substrate was calculated with them by applying the initial and boundary conditions mentioned earlier. A required condition is the heat flux per unit area, q, appearing in the finite difference approximation for Node 1 in Table 2 and in Eq. 8. In this work, this heat flux was evaluated by solving an inverse heat conduction problem using a sequential function specification method [35] and a brief account is given here. The entire period in which heat transfer is calculated is divided into a finite number of time intervals. The heat flux varies from one interval to another but a constant value, q_m, is assumed within each individual interval, 'm'. The optimized value of the heat flux is obtained by iteration using the following formula:

$$q_m^{n+1} = q_m^n + \frac{\sum_{i=1}^{r}\sum_{j=1}^{J}\left(Y_{m+i-1,j} - T_{m+i-1,j}\right)\cdot Z_{i,j}^n}{\sum_{i=1}^{r}\sum_{j=1}^{J}\left(Z_{i,j}^n\right)^2} \tag{9}$$

where $Z_{i,j}^n$ is a sensitivity coefficient defined as:

$$Z_{i,j}^n \approx \frac{T_{m+i-1,j}\left(q_m^n(1+\delta)\right) - T_{m+i-1,j}\left(q_m^n\right)}{\delta\, q_m^n} \tag{10}$$

The subscripts r and J refer, respectively, to the number of future time steps and the number of thermocouples used to calculate the heat flux ($J = 1$ in this study). The former is used to increase the stability of the iterative process; it was usually equal to 3 or 4 in this study. $Y_{m+i-1,j}$ is the measured temperature at the time interval $m + i - 1$ and $T_{m+i-1,j}$ is the calculated temperature using the explicit finite-difference equations in Table 2. Equation 9 was used iteratively using a start value for q_m^n until the following convergence condition was met:

$$\frac{q_m^{n+1} - q_m^n}{q_m^n} \le 0.005 \tag{11}$$

At this point the flux, q_m^n, required to produce the measured temperature, $Y_{m,j}$ was obtained. Since explicit finite difference approximations were used, the time steps and spatial discretization were subjected to the dimensionless Fourier and Biot numbers. The accuracy of the calculations produced by this algorithm was verified against the exact solution of a triangular heat flux problem [35]. The agreement between the two is illustrated in Fig. 2.

Table 1 Thermophysical properties of copper and aluminum

	Reference
Copper	
$C = 4.77 \times 10^{-1} - 1.68 \times 10^{-4}T - 5.07 \times 10^{3}T^{-2} + 1.49 \times 10^{-7}\mathrm{T}^2$ (kJ kg^{-1} K^{-1})	[30]
$k = 419 - 6 \times 10^{-2}T$ (W m^{-1} K^{-1})	[31]
$\rho = 8920$ (kg m^{-3})	[32]
Aluminum	
$\gamma = 0.881$ (N m^{-1})	[33]
$\sigma = 0.881$ (J m^{-2})	[33]
$\rho = 2368$ (kg m^{-3})	[32]

Table 2 Explicit finite difference temperature approximations derived from Eq. 2 [34]

Node	Substrate temperature
1	$T_1^{p+1} = T_1^p + \frac{2k_1^p\Delta t}{\rho C_1^p \Delta x^2}\left[\left(T_2^p - T_1^p\right) + \frac{q^p\Delta x}{k_1^p}\right] + \frac{\mathrm{d}k}{\mathrm{d}T}\frac{\Delta t}{\rho C_1^p}\left(\frac{q^p}{k_1^p}\right)^2$
I	$T_i^{p+1} = T_i^p + \frac{k_i^p\Delta t}{\rho C_i^p \Delta x^2}\left[\left(T_{i+1}^p - 2T_i^p + T_{i-1}^p\right) + \frac{\mathrm{d}k}{\mathrm{d}T}\frac{1}{4k_i^p}\left(T_{i+1}^p - T_{i-1}^p\right)^2\right]$
N	$T_N^p = T_{\mathrm{Measured}}^p$

Experimental procedure

The experimental set-up that was constructed is depicted in Fig. 3 and closely resembled that of Ebrill et al. [5–8] and

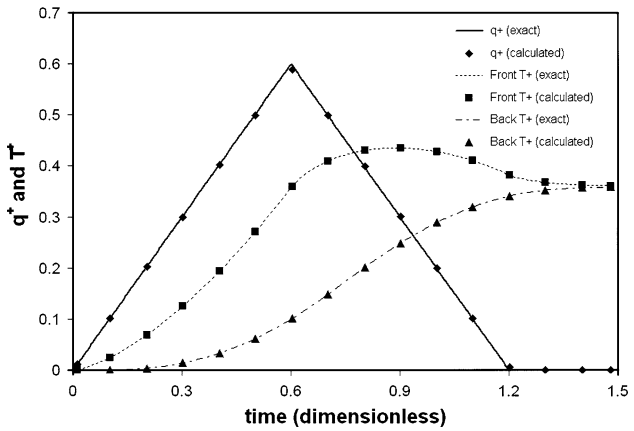

Fig. 2 Dimensionless heat flux (q^+) as function of dimensionless time (t^+) for a triangular heat flux imposed at the surface of a finite insulated plate. The front and back dimensionless temperatures (Front T^+ and Back T^+) as a function of dimensionless time are also shown for the plate. Greater details are given in reference [35]

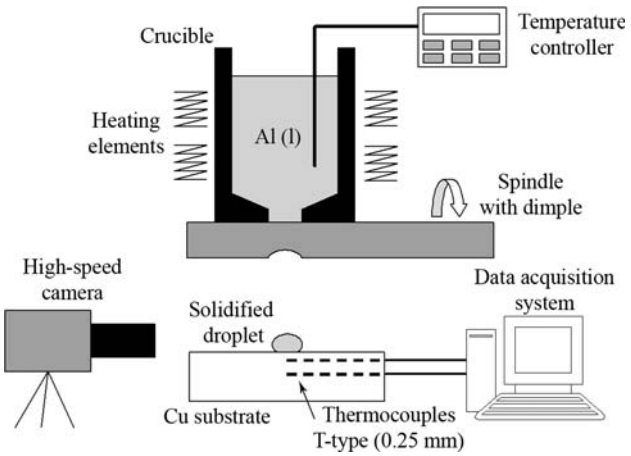

Fig. 3 Drop-splat experimental set-up for the simultaneous characterization of dynamic wetting and heat transfer at the initiation of solidification of aluminum

Todoroki et al. [20–22]. Typically, 200 g of aluminum were melted and held at 725 °C in the graphite crucible (155 mm high, 75 mm in diameter) using electrical resistance heating elements. Two aluminum alloys were used in this study: AA1070 (99.7 wt.% Al, commercially pure aluminum) and AA5754 (in wt.%: 3.41 Mg, 0.14 Mn, 0.07 Si, 0.18 Fe, 0.015 Ti, 0.009 V, 0.004 Cu, Bal. Al). An electric motor was used to rotate the spindle (75 mm long, 25 mm in diameter) in which a dimpled cavity was machined. As it faced the small hole at the bottom end of the crucible, this cavity was filled with liquid aluminum and a molten droplet was formed following the rotation of the spindle. The crucible, spindle, and electric motor, rested on a table that allowed a displacement in the x, y, and z directions for adjusting the position of the droplet with respect to the substrate. The size of the dimple in the spindle depended on the desired droplet mass. The results presented in this paper were obtained with droplets whose diameters were between 5.1 and 7.4 mm and masses ranging from 0.17 to 0.51 g. The height of fall was between 10 and 12 mm and the velocities at impact were between 0.44 and 0.49 m/s.

During an experiment, the droplet was released under free-fall conditions, impinged on the copper substrate and solidified. To record the temperatures in the substrate, type-T thermocouples (copper–constantan) were used. The constantan lead wire (0.125 mm diameter) was shielded with a stainless steel sleeve containing a ceramic insulator (0.8 mm diameter) and inserted into a drilled hole (1 mm diameter) that reached the mid width of the substrate. It was held in contact with the bottom of the drilled hole using a spring to ensure good contact. A copper lead wire was also screwed directly to the back of the substrate to complete the thermocouple. This arrangement was semi-intrinsic as the substrate acted as one element of the circuit [24, 25, 36]. Two such thermocouples were used in the tests, one at a depth of approximately 1 mm from the surface, the other at 5 mm, the exact location being measured to a precision of 0.01 mm with a vernier prior to an experimental run. Figure 4 illustrates the thermocouple arrangement in the substrate. The temperatures were measured at a frequency of 1000 Hz.

The substrates (50 × 120 × 20 mm^3) consisted of electrolytic tough pitched, ETP, copper with a purity of 99.9+% and held in place with a vice. Two surface finishes were investigated; the first obtained by polishing up to a 600 grit paper that produced an arithmetical average roughness (R_a) of 0.2 μm and a waviness spacing of 1.58 mm, the second

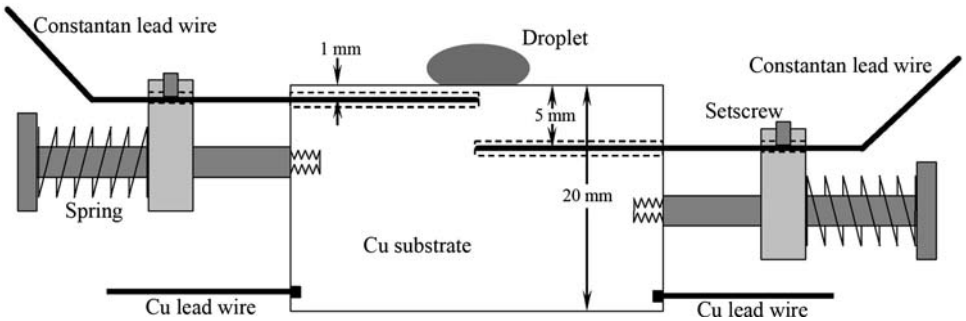

Fig. 4 Schematic of the thermocouple arrangement in the substrate

obtained by sand blasting that produced a roughness (R_a) of 6.4 μm and a waviness spacing of 7.37 mm. The roughness and waviness measurements were performed according to the ASME B46.1-2002 standard using an optical profilometer (model CHR 450, STIL Inc.). Several experimental campaigns were carried out with the substrates and their surface finishes were reconditioned by performing the polishing or sand-blasting procedures over again. Target lines were drawn on the substrate to adjust the fall of the droplet directly above the hot junction of the thermocouples. Experiments with off-centered splats were discarded from the heat transfer analysis.

The high-speed camera (Fastcam-PCI Photron, CCD detector, 256 × 240 bit resolution at 1000 frames/s, Tamron objective 28–105 mm) captured the evolution in the shape of the droplet as it spread on the substrate. The camera could record images up to 10,000 frames/s, but the operating frequency was set to 1,000 frames/s. The whole set-up was enclosed in an aluminum chamber that could provide a controlled atmosphere. An acrylic window covered the front of the chamber and provided the observation porthole for the high-speed camera. A gauntlet was also used to manipulate the set-up inside the chamber when a controlled atmosphere was used. The chamber was not perfectly gastight but a positive pressure was provided. Tests were performed in ambient air as well as in argon (99.998%, BOC Canada Ltd.) and helium (99.999%, BOC Canada Ltd.). An oxygen detector (model IR 2200, Infrared Industries Inc.) was used to measure the oxygen concentration in the chamber when argon and helium were used. An attempt was also made to evaluate the degree of surface oxidation in preheated copper substrates by measuring the proportion of oxygen using an energy-dispersive X-Ray spectroscopy system (Oxford INCA 300) mounted on a scanning electron microscope (Hitachi SU-70 FEGSEM).

Results and discussion

Figure 5 provides a series of pictures illustrating a typical spreading of the droplet impinging on a substrate. The droplet first impacted the substrate and then spread out on it. The spreading generally took 3–10 ms to be fully established after which, it remained constant. The free surface of the droplet however oscillated for approximately 0.35 s.

Using the height of fall and the mass for the droplet given in the figure caption and also using the data in Table 1, a Weber number of 3.5 is obtained while the ratio of the kinetic energy to surface energy is 0.29. In all the experiments presented in this paper, these values remained fairly constant and varied by about 10% or less. Caution must however be used in the interpretation of these ratios since during free fall the droplets reacted with oxygen in the gaseous atmosphere and this may have affected surface tension. Extremely low partial pressures of oxygen are required to prevent the reaction of liquid aluminum with oxygen to form aluminum oxide, Al_2O_3. Using the standard free energy change for this reaction [37], an oxygen partial pressure close to 10^{-50} bar is required to prevent the formation of aluminum oxide at 725 °C. The rate of formation of metal oxides has been discussed elsewhere (see [32] for example) and it is beyond the scope of this work to estimate the thickness of the aluminum oxide skin in these experiments but it is reasonable to assume that an oxide layer was always present. It has been reported that such a layer could increase the 'apparent' surface tension up to 100 times [16]. This layer may not only affect spreading of the aluminum on the substrate but also the heat transfer since it acts as a thermal resistance. It should be realized that copper readily oxidizes and an oxygen partial pressure close to 10^{-50} bar is also required to prevent the formation of Cu_2O at 298 °C [37]. The presence of oxide layers at the surface of liquid aluminum and metallic substrates is prevalent in virtually all metallurgical processes that involve wetting and solidification and the experimental tests were thus carried out in comparable environments.

Figure 6 is a photomicrograph of a solidified droplet showing the chill zone at the bottom where solidification was initiated upon contact with the substrate. Columnar grains are apparent and a shrinkage pipe also formed at the

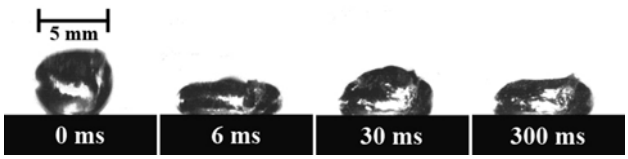

Fig. 5 Spreading for a droplet on a substrate. Tests carried out with AA1070 aluminum in ambient air, polished substrate ($R_a = 0.2$ μm and waviness spacing of 1.58 mm). Height of fall: 10.0 ± 0.5 mm. Droplet mass: 0.353 ± 0.005 g, spreading factor: 1.23 ± 0.05, uncertainties refer to one standard deviation of the mean. $We = 3.5$, $E_K/E_{surf} = 0.29$, $v = 0.44$ m/s, $d = 6.6$ mm

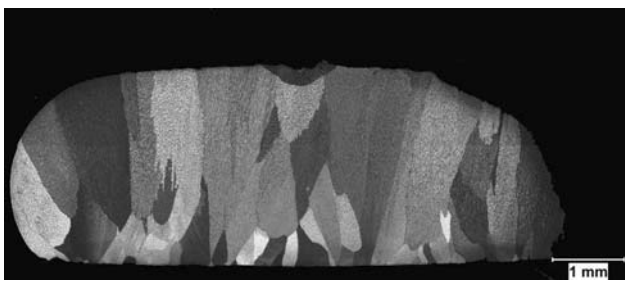

Fig. 6 Photomicrograph of an aluminum droplet obtained by electrolytic etching showing a grain structure that formed under unidirectional heat flow solidification

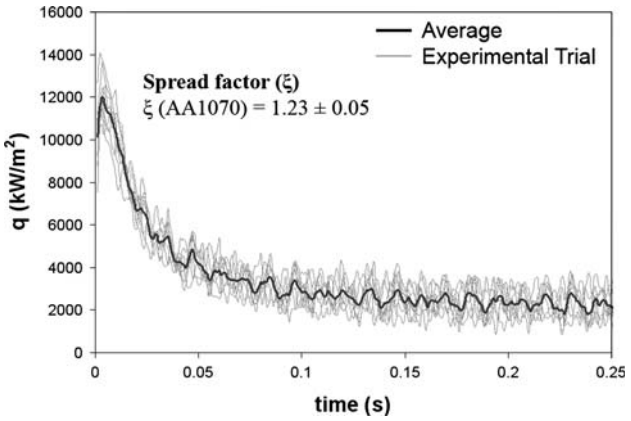

Fig. 7 Heat flux curves and average spreading factor obtained for a set of eight droplets. Tests carried out with AA1070 aluminum in ambient air, polished substrate ($R_a = 0.2$ μm and waviness spacing of 1.58 mm). Height of fall: 10.0 ± 0.5 mm. Droplet mass: 0.353 ± 0.005 g. $We = 3.5$, $E_K/E_{surf} = 0.29$, $v = 0.44$ m/s, $d = 6.6$ mm

center top of the droplet. The orientation of the columnar grains indicates that heat transfer was unidirectional and solidification thus proceeded from bottom to top with a temperature gradient in that direction. The temperature in the droplet was therefore not homogeneous and this affected how heat evolved. This was implicitly accounted by the temperature measurements and inverse heat flux calculations that ensued.

Typical heat flux results for eight trials (eight droplets) are shown in Fig. 7 for the same experimental conditions given in the caption of Fig. 5. Good reproducibility was obtained since all the heat flux curves were within 10–15% of the calculated average. The heat flux curves presented in subsequent figures are average values for a minimum of five trials. The curves in Fig. 7 show that a highly transient regime took place during the first 50 ms. The two physical phenomena that have been attributed to this regime are contact of the liquid metal with the substrate and nucleation of crystals [38–40]. After 50 ms, the heat flux is considerably reduced and the variation is small. This steadier behavior has been associated with the presence of an interfacial gap as the solidified skin contracts away from the substrate [40–43]. Consequently, an arbitrary cut-off was used in the analysis of the heat fluxes and those occurring before and after 50 ms were analyzed separately. It should be noted that the areas under these curves, $\int q\,dt$, refer to the amount of heat per unit area transferred to the substrate and have the units of J/m^2. At 725 °C, the heat content of the AA1070 alloy is 1146 kJ/kg [44] or 405 J for the 0.353 g droplets of Fig. 5. Assuming that heat losses of the droplet by convection and radiation are negligible and that heat flow in the substrate is entirely unidirectional, an estimate of the solidification time can be made by integrating the heat fluxes over time given in Fig. 7 and multiplying by the contact area of the droplet (4.7×10^{-5} m^2). Assuming a constant heat flux value of 1730 kW/m^2 after 0.25 s, the droplet reaches its solidus temperature of 646 °C and heat content of 683 kJ/kg [44] after 1.8 s. Although this is a rough estimate of the solidification time, it illustrates that larger fluxes in a given amount of time will provide a greater cooling efficiency and a more rapid solidification. An alternative method to estimate cooling efficiency would be to evaluate the time required for the droplet to transfer its superheat to the substrate. The removal of superheat however occurs so rapidly in these experiments that the response time of the thermocouples would need to be accounted for an accurate evaluation. Accounting for the thermocouple response time would also be useful to correlate wetting with the Stefan number (the ratio of the sensible heat content to the latent heat content) and to compare the variations of the droplet contact radius with the heat flux. Also shown in Fig. 7 is the average spreading factor and it is seen that the reproducibility was good. The roles that alloy composition, initial temperature of the substrate, surface roughness of the substrate, and gaseous atmosphere have on spreading and heat flow are discussed in the next sections.

Effect of droplet composition

As mentioned in a previous section, the tests were performed with aluminum at two different compositions, the first with 99.7 wt.% aluminum (AA1070), the second containing close to 96.5 wt.% aluminum and 3.5 wt.% magnesium (AA5754). Their spreading factors and heat flux results are shown in Fig. 8. A better spreading was observed with the AA5754 alloy ($\xi = 1.8$) than with the AA1070 ($\xi = 1.22$). Magnesium is known to decrease the

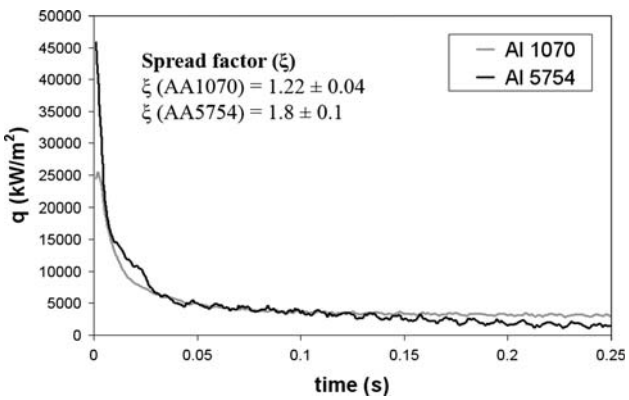

Fig. 8 Differences in the spreading factors and the heat flux evolution for the AA1070 and AA5754 alloys. Tests carried out in ambient air on polished substrate ($R_a = 0.2$ μm and waviness spacing of 1.58 mm) initially at room temperature. Height of fall: 10.0 ± 0.5 mm. Droplet mass: 0.508 ± 0.005 g. $We = 3.9$, $E_K/E_{surf} = 0.33$, $v = 0.44$ m/s, $d = 7.4$ mm

surface tension of aluminum by acting as a surface-active element [45] and it is here considered to be the main reason for the improved spreading. It should nevertheless be noted that with the AA1070 aluminum, the oxide skin around the droplet was mainly composed of aluminum oxide, Al_2O_3, whereas with the AA5754 alloy this Al_2O_3 skin may have been mixed with MgO. As discussed earlier, the effect of oxide skins must not be overlooked in both wetting and heat transfer and differences in the chemical compositions not only apply to the droplet alloys but also to the oxide skins.

The improved wetting for the AA5754 alloy was accompanied with a substantially larger initial heat flux as seen in Fig. 8. This heat flux underwent a sharp decrease with time of contact. After approximately 50 ms, both alloys exhibited heat fluxes that were nearly the same.

Effect of initial substrate temperature

Trials with initial substrate temperatures of 80 °C, 175 °C, and 275 °C were carried out. The surfaces of the substrates at 80 °C and 175 °C retained their shinny luster but those at 275 °C were darker and lackluster. A chemical analysis at the surface of the substrates performed by EDS showed that the oxygen contents for the three temperatures were respectively 0.21%, 13.33%, and 27.27%. The relatively high value obtained at 275 °C is a good explanation for the lackluster appearance. The heat fluxes and the spreading factors obtained at these three initial temperatures are shown in Fig. 9. The heat per unit area transferred to the substrate during the first 50 ms also increased from 80 °C to 175 °C but then substantially decreased at 275 °C. The greater surface oxidation of the substrate at 275 °C may have increased the thermal resistance and caused the heat flow to diminish. After approximately 50 ms, the substrate at 275 °C however possessed the largest heat flux and this could be caused by a greater adherence between the aluminum and the substrate at this temperature. Sticking of the droplets on the substrates after an experiment was not noticed although adherence was not a factor that was evaluated. The spreading factors given in Fig. 9 show that increasing the initial substrate temperature provided an improvement in dynamic wetting. Typically, wetting in metal/metal systems is superior to metal/oxide systems but there are instances where this trend is reversed for reactive metal/oxide systems [16].

Effect of surface roughness

Two different surface finishes were produced for the substrates; a smooth surface obtained by polishing with a 600 grit paper and a rough surface obtained by sand blasting. Their arithmetical average roughness (R_a) was, respectively, 0.2 and 6.4 μm and the waviness spacing were 1.58 and 7.37 mm. The results obtained with these surface conditions are shown in Fig. 10. The spreading factors were the same but the heat flux during the first 50 ms was significantly higher for the polished substrate. After this period, the fluxes in both substrates were nearly the same. The rough surface texture consisted of higher peaks and deeper valleys and the surface tension of the droplet may have prevented a proper contact inside the valleys. The reduction in the interfacial contact surface area with rough surfaces has been reported to be the cause of the lower heat flows in other studies [46, 47]. In terms of spreading, the

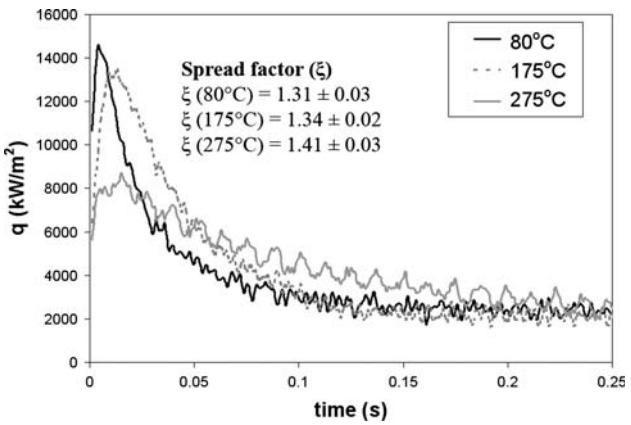

Fig. 9 Differences in the spreading factors and the heat flux evolution for the AA1070 alloy at different initial substrate temperatures. Tests carried out in ambient air on polished substrate (R_a = 0.2 μm and waviness spacing of 1.58 mm). Height of fall: 10.0 ± 0.5 mm. Droplet mass: 0.406 ± 0.005 g. We = 3.6, E_K/E_{surf} = 0.30, v = 0.44 m/s, d = 6.9 mm

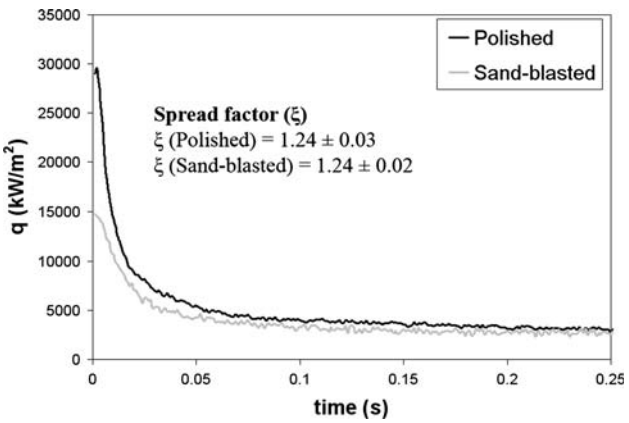

Fig. 10 Differences in the spreading factors and the heat flux evolution for the AA1070 alloy for two substrate surface finish (polished = 0.2 μm R_a, waviness of 1.58 mm, and sand blasted = 6.4 μm R_a, waviness spacing of 7.37 mm). Tests carried out in ambient air on substrates initially at room temperature. Height of fall: 10.0 ± 0.5 mm. Droplet mass: 0.511 ± 0.006 g. We = 3.9, E_K/E_{surf} = 0.33, v = 0.44 m/s, d = 7.4 mm

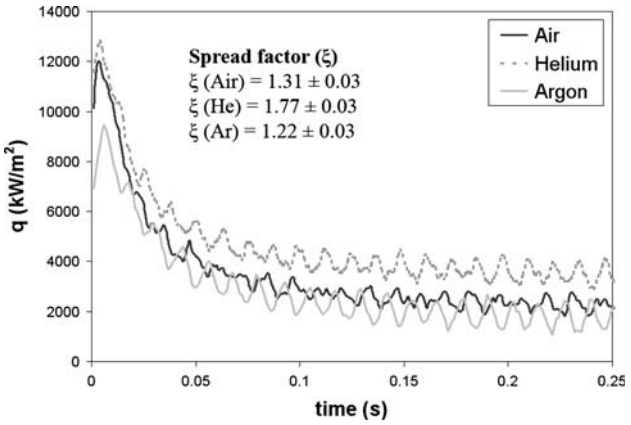

Fig. 11 Differences in the spreading factors and the heat fluxes for the AA1070 alloy in ambient air, argon (0.2% O_2), and helium (0.2% O_2). Tests carried out on polished substrates ($R_a = 0.2$ μm, waviness of 1.58 mm) initially at room temperature. Height of fall: 10.0 ± 0.5 mm. Droplet mass: 0.352 ± 0.004 g. $We = 3.9$, $E_K/E_{surf} = 0.29$, $v = 0.44$ m/s, $d = 6.6$ mm

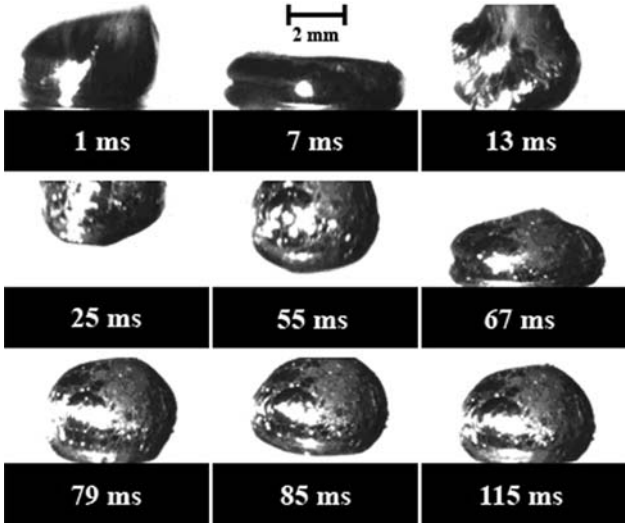

Fig. 12 Aluminum droplet impinging, spreading, and bouncing back from the substrate in an argon atmosphere (0.02% O_2). Tests carried out on polished substrates ($R_a = 0.2$ μm, waviness spacing of 1.58 mm) initially at room temperature. Height of fall: 12.0 ± 0.5 mm. Droplet mass: 0.17 ± 0.05 g. Spreading factor: 1.05 ± 0.02. $We = 3.3$, $E_K/E_{surf} = 0.27$, $v = 0.48$ m/s, $d = 5.1$ mm

reduction in contact surface area combined with gas trapped in the valleys and the greater waviness spacing may also have allowed the droplet to spread as well as on the smooth surface.

Effect of gaseous atmospheres

The effect of the gaseous atmosphere on spreading and heat flow was investigated with ambient air, argon, and helium. The experiments with the inert gases were carried out by purging the ambient air from the chamber containing the experimental set-up. An oxygen sensor was inserted in the chamber and a series of tests were conducted with a residual amount of oxygen of 0.2% in the argon and helium. The results with the three gases are shown in Fig. 11. The spreading factors were the highest for helium followed by air and argon and the heat fluxes during the first 50 ms after impingement followed the same order. After 50 ms, the heat fluxes with helium remained the highest while those for air and argon were close to one another. The thermal diffusivity of helium being almost one order of magnitude greater than that of air and argon [48], it is plausible that the presence of a layer of gas trapped at the substrate/droplet interface provided the improved heat flow. Heat loss to the gas phase during free fall could have been greater when helium was used but this effect seems negligible since the droplet transferred the greatest amount of heat to the substrate during the time shown in the figure.

Additional experiments were performed with argon in the chamber having a residual oxygen level reduced to 0.02% O_2. Under these conditions the aluminum droplet exhibited a considerably different behavior. As shown in Fig. 12, the droplet impinged on the substrate (1 ms),

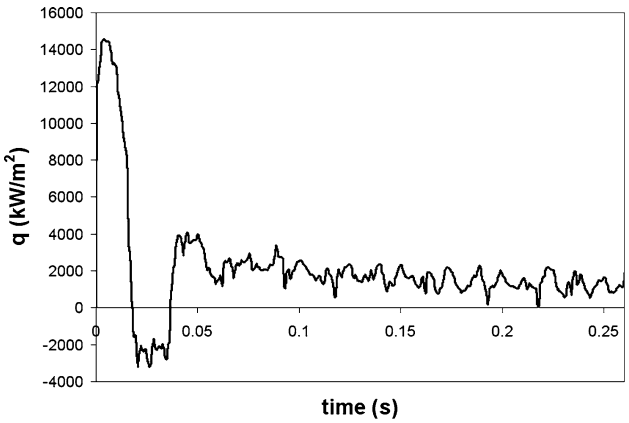

Fig. 13 Heat flow evolution at the surface of the substrate for a droplet (AA1070 alloy) in an argon atmosphere (0.02% O_2) impinging, spreading, and bouncing back from the substrate. As the droplet bounced back, the substrate cooled and the flux became negative. The trial was carried out on a polished substrate ($R_a = 0.2$ μm and waviness spacing of 1.58 mm) initially at room temperature. Height of fall: 12.0 ± 0.5 mm. Droplet mass: 0.34 ± 0.05 g. Spreading factor: 1.05 ± 0.02. $We = 4.1$, $E_K/E_{surf} = 0.34$, $v = 0.48$ m/s, $d = 6.5$ mm

spread (7 ms), and then bounced away from the substrate (13, 25, and 55 ms). The droplet repeated this sequence (67, 79, and 85 ms) before coming to rest at 115 ms with a spreading factor of 1.05. This behavior was observed with droplets having masses between 0.17 and 0.34 g. The Weber numbers varied between 3.3 and 4.1 and the E_K/E_{Surf} ratios ranged between 0.27 and 0.34. The heat

flux obtained with a droplet in this atmosphere is shown in Fig. 13. As the droplet bounced for the first time, the surface of the substrate cooled and this is shown by the heat flux becoming negative. The droplets from the previous tests performed in the Ar–0.2% O_2 atmosphere did not bounce even though the Weber number and E_K/E_{Surf} ratio was within this range. It can also be observed that the spreading factors in the Ar–0.02% O_2 atmosphere are the lowest of all those obtained in this study. It is possible that the reduction of the oxygen potential modified the oxide skin from a continuous to a discontinuous film. This may have yielded a reduction in wetting in a similar manner as what has been reported with the coated water droplets [49]. The authors of this study reported that the wetting of these droplets on glass was suppressed by coating them with a monolayer of hydrophobic powder. In addition, Matson et al. [29], in their work on spray processing of aluminum, developed an impingement map to classify a variety of impact categories. Droplet rebounds were observed to occur at relatively low Weber numbers (between 1 and 100) and Freezing numbers greater than 100. The latter dimensional number was derived by the authors to relate the time to solidify and the time to impact. More work is required to evaluate the effect of the oxide skins for the droplets produced with the present drop-splat experiments and impingements maps offer an interesting avenue to provide a greater understanding of the wetting and heat transfer phenomena.

Table 3 provides qualitative comparisons of the effects of the experimental conditions on the spreading factors and the heat fluxes. There are two columns for the heat fluxes, one for the transient regime ($t < 50$ ms) and the other for the steady-state regime ($t > 50$ ms). The comparisons are with respect to an AA1070 aluminum droplet at 725 °C in air and impinging a copper substrate at 25 °C having a surface roughness of 0.2 μm R_a and a waviness spacing of 1.58 mm. It is seen from the table that a positive correlation between the spreading factors and transient heat fluxes was observed when the surface tension of the alloy was decreased, the substrate surface temperature was increased up to 175 °C, the diffusivity of the gaseous atmosphere was increased, and the level of oxygen in argon was reduced to 0.02% O_2. This positive correlation was not observed when the initial substrate temperature was 275 °C and when the substrate surface roughness and waviness spacing were increased. In the first case, the greater surface oxidation of the substrate observed at 275 °C may have increased the thermal resistance, causing the heat flow to diminish. In the second case, gas trapped in the asperities at the surface of the substrate may have acted as a cushion that promoted spreading while decreasing the effective contact area for heat flow conduction.

Table 3 also shows that the spreading factors and the steady-state heat fluxes ($t > 50$ ms) are more difficult to correlate. This may be caused by the fact that spreading was typically completed before the steady-state heat flow was established. Spreading factors and steady-state heat fluxes however both increased at an initial substrate temperatures of 275 °C but the increase in heat flux may have been caused by a greater adherence of the droplet on the substrate that diminished the size of the interfacial gap. Spreading factors and steady-state heat fluxes also both increased in the presence of greater gas diffusivity. This may be also attributed to the interfacial gap since it would be filled with gas.

Table 3 Summary of effects of experimental conditions on spreading factors and heat fluxes

Experimental conditions	Spreading factors	Transient heat fluxes ($t < 50$ ms)	Steady-state heat fluxes ($t > 50$ ms)
1. Alloy composition			
Alloy surface tension ↓	↑	↑	=
2. Substrate temperature ↑			
$T \leq 175$ °C	↑	↑	=
$T = 275$ °C	↑	↓	↑
3. Substrate roughness ↑	=	↓	=
4. Gas composition			
Diffusivity of gas ↑	↑	↑	↑
O_2 level in Ar ↓	↓	↓	=

The increase (↑), decrease (↓), or equal (=) are with respect to a AA1070 aluminum droplet at 725 °C in air and impinging a copper substrate at 25 °C having a surface roughness of 0.2 μm R_a and a waviness spacing of 1.58 mm

Conclusions

Drop-splat experiments with aluminum alloy droplets solidifying on copper substrates were carried to examine the relationship between dynamic wetting and heat transfer under various experimental conditions. The results showed that an improvement in the dynamic wetting was often accompanied by an increase in the heat transfer, especially in its early stages, but the relationship was not systematic. It was postulated that factors such as variations in the oxidation at the surface of the substrates and the droplets as well as gas trapped at the interface between the droplet and the substrate affected any relationship.

Acknowledgements Technical assistance from Daniel Simard, Christian Corbeil, Hugues Blanchette. Geneviève Simard, Hélène Grégoire, and Marie-Ève Larouche from the Aluminum Technology Center are acknowledged. The authors would also like to thank Centre québécois de recherche et de développement de l'aluminium (CQRDA) and Fond québécois de la recherche sur la nature et les technologies (FQRNT) for their financial support.

References

1. Dong S, Niiyama E, Anzai K (1994) Mater Trans JIM 35:196
2. Jacobson LA, McKittrick J (1994) Mater Sci Eng R 11:355
3. Adler PI, Hsu SC (1983) In: Mehrabian R (ed) Rapid solidification processing: principles and technologies, vol 3. Taiwan Institute of Technology, Taiwan, p 448
4. Maringer RE (1988) Mater Sci Eng 98:13. doi:10.1016/0025-5416(88)90117-6
5. Ebrill N (2000) PhD Thesis University of Newcastle, Callaghan, Australia
6. Ebrill N, Durandet Y, Strezov L (2001) Trans JWRI Jpn 30:351
7. Ebrill N, Durandet Y, Strezov L (2001) Verlag Stahleisen GMBH, Galvatech, p 329
8. Ebrill N, Durandet Y, Strezov L (2000) Metall Mater Trans B 31B:1069. doi:10.1007/s11663-000-0082-3
9. Ulrich J, Berg M, Bauckhage K (1999) In: Mishra B (ed) EPD Congress, The Minerals, Metals & Materials Society,Warrendale, p 105
10. Amada S, Haruyama M, Ohyagi T, Tomoyasu K (2001) Surf Coat Tech 138:211. doi:10.1016/S0257-8972(00)01077-X
11. Nishioka E, Matsubara T, Fufumoto M (2001) Int J Mater Prod Technol SPM1 (Special Issue):700
12. Fukai J, Asami H, Miyatake O (1998) Minerals, Metals and Materials Society/AIME, Warrendale, p 473
13. Megaridis CM, Boomsma K, Bayer IS (2004) Fluid Mech Transp Phenom 50:1356
14. Schiaffino S, Sonin AA (1997) Phys Fluids 9:2217. doi:10.1063/1.869344
15. Rioboo R, Adao MH, Voué M, De Coninck J (2006) J Mater Sci 41:5068. doi:10.1007/s10853-006-0445-5
16. Eustathopoulos N, Nicholas MG, Drevet B (1999) Wettability at high temperatures. Pergamon, New York
17. Liu W, Wang GX, Matthys EF (1992) HTD 196:111
18. Liu W, Wang GX, Matthys EF (1995) Int J Heat Mass Transfer 38:1387. doi:10.1016/0017-9310(94)00262-T
19. Wang GX, Matthys EF (1994) In: Proceedings of the 10th international heat transfer conference, 1994. IchemE Pub, Brighton, p 169
20. Todoroki H, Lertarmon R, Cramb AW, Suzuki T (1999) Iron Steelmaker 26:57
21. Todoroki H, Lertarmon R, Suzuki T, Cramb AW (1997) In: 80th Steelmaking conference proceedings, 1997. Iron and Steel Society/AIME, Warrendale, p 667
22. Todoroki H, Lertarmon R, Suzuki T, Cramb AW (1997) Minerals, Metals and Materials Society/AIME, Warrendale, p 2227
23. Misra P, Phininchka N, Cramb AW (2003) In: ISSTech 2003 conference proceeding. Iron and Steel Society/AIME, Warrendale, p 263
24. Loulou T, Artyukhin EA, Bardon JP (1999) Int J Heat Mass Transfer 42:2129. doi:10.1016/S0017-9310(98)00338-X
25. Loulou T, Bardon JP (2000) High Temp Mater Process 4:69
26. Evans T, Strezov L (2000) Metall Mater Trans B 31B:1081. doi:10.1007/s11663-000-0083-2
27. Leboeuf S, Bouchard D, Nadeau JP, Guthrie RIL, Isac M (2003) In: Masounave J, Dufour G (eds) Proceedings of the international symposium on light metals 2003 Métaux Légers, CIM, Montreal, p 215
28. Massey BS (1989) Mechanics of fluids, 6th edn. Van Nostrand Reinhold Int, London, UK
29. Matson DM, Rolland M, Flemings MC (1998) Solidification 1998. The Minerals, Metals and Materials Society/AIME, Warrendale, p 389
30. Kubaschewski O, Alcock CB, Spencer PJ (1993) Materials thermochemistry, vol 6. Pergamon Press Ltd, New York, p 274
31. Touloukian YS, Powell RW, Ho CY, Klemens PG (1970) Thermophysical properties of matter, vol 1. Plenum Publishing Corp, New York, p 81
32. Poirier DR, Geiger GH (1994) Transport phenomena in materials processing. The Minerals Metals and Materials Society, Warrendale, USA
33. Egry I, Schneider S, Seyhan I, Volkmann T (2001) Trans JWRI 30:195
34. Li G, Thomas BG (1996) Metall Mater Trans B 27B:509. doi:10.1007/BF02914916
35. Beck JV, Blackwell B, St. Clair CR (1985) Inverse heat conduction. Wiley-Interscience Publication, New York
36. Bouchard D, Howes B, Paumelle C, Nadeau JP, Simard D (2002) Metall Mater Trans B 33B:403. doi:10.1007/s11663-002-0052-z
37. Gaskell DR (1981) Introduction to metallurgical thermodynamics, 2nd edn. McGraw-Hill Book Co., New York
38. Nishida Y, Drosti W, Engler S (1986) Metall Trans 17B:833
39. Wang G-X, Matthys EF (1994) In: Proceedings of the 10th international heat transfer conference. IchemE Pub.,UK, p 169
40. Strezov L, Herbertson J (1998) Iron Steel Inst Jpn Int 38:959
41. Pehlke RD (1995) Modeling of casting, welding and advanced solidification processes VII. TMS, Warrendale, PA, p 373
42. Ho K, Pehlke RD (1985) Metall Trans B 16B:585
43. Ho K, Pehlke RD (1983) AFS Trans 91:689
44. Thermo-Calc Windows version 4, Stockholm, Sweden, 2006
45. Lang G (1974) Aluminum 50–51:731
46. Muojekwu CA, Samarasekera IV, Brimacombe JK (1995) Metall Mater Trans B 26B:361. doi:10.1007/BF02660979
47. Prates M, Biloni H (1972) Metall Trans 3:1501. doi:10.1007/BF02643039
48. Bejan A, Kraus AD (2003) Heat transfer handbook. John Wiley & Sons, Inc., Hoboken, NJ, p 151
49. Aussillous P, Quéré D (2001) Nature 411:924. doi:10.1038/35082026